

γ -ray emission from the Westerlund 1 region

S. Ohm,¹ J.A. Hinton¹ and R. White¹

¹ *Department of Physics and Astronomy, The University of Leicester, University Road, Leicester, LE1 7RH, United Kingdom*

Accepted 2013 June 24. Received 2013 June 21; in original form 2013 May 02

ABSTRACT

Westerlund 1 (Wd 1) is the most massive stellar cluster in the Galaxy and associated with an extended region of TeV emission. Here we report the results of a search for GeV γ -ray emission in this region. The analysis is based on ~ 4.5 years of *Fermi*-LAT data and reveals significantly extended emission which we model as a Gaussian, resulting in a best-fit sigma of $\sigma_S = (0.475 \pm 0.05)^\circ$ and an offset from Wd 1 of $\sim 1^\circ$. A partial overlap of the GeV emission with the TeV signal as reported by H.E.S.S. is found. We investigate the spectral and morphological characteristics of the γ -ray emission and discuss its origin in the context of two distinct scenarios. Acceleration of electrons in a Pulsar Wind Nebula provides a reasonably natural interpretation of the GeV emission, but leaves the TeV emission unexplained. A scenario in which protons are accelerated in or near Wd 1 in supernova explosion(s) and are diffusing away and interacting with molecular material, seems consistent with the observed GeV and TeV emission, but requires a very high energy input in protons, $\sim 10^{51}$ erg, and rather slow diffusion. Observations of Wd 1 with a future γ -ray detector such as CTA provide a very promising route to fully resolve the origin of the TeV and GeV emission in Wd 1 and provide a deeper understanding of the high-energy (HE) astrophysics of massive stellar clusters.

Key words: radiation mechanisms: non-thermal, diffusion, gamma-rays: ISM

1 INTRODUCTION

Supernova remnants (SNRs) have long been suggested as the dominant source of Galactic cosmic rays (GCRs). The massive progenitor stars of these supernova (SN) explosions are usually bound in associations or stellar clusters and shape their immediate surroundings with their fast supersonic winds or in interactions with the winds and/or shockwaves of already exploded member stars. In this way a *superbubble*, filled with a hot tenuous plasma, can form. In such a system particles may be accelerated by supersonic turbulences and/or via repeated diffusive shock acceleration to TeV energies and beyond (e.g. Bykov 2001; Parizot et al. 2004). γ -ray observations from hundreds of MeV to multi-TeV energies with satellite instruments and using ground-based Cherenkov telescopes are an ideal tool to study not only the acceleration sites of GCRs, but also their interaction with and transport in the surrounding interstellar medium (ISM). Stellar clusters and superbubbles are emerging as a new source population in the γ -ray band. Associations include the non-thermal emission from the Cygnus region (Aharonian et al. 2005; Ackermann et al. 2011) and the TeV emission from the young massive stellar clusters Westerlund 2 and Westerlund 1 (Wd 1) (Aharonian et al. 2007; Abramowski et al. 2011, 2012). These observations suggest that the collective effect of stellar winds and/or past SN activity in these complexes indeed results in a significant production of GCRs.

Wd 1 is the most massive stellar cluster in the Milky Way with a total mass between $\sim 5 \times 10^4 - 10^5 M_\odot$ (Clark et al. 2005; Lim

et al. 2013) and a very rich population of post main sequence stars (e.g. Clark & Negueruela 2002). Distance estimates over the past ten years seem to converge to 4.0–5.0 kpc, and we will employ the ~ 4.3 kpc as used by Abramowski et al. (2012) in the following. The age estimate of the stellar cluster of ~ 4 Myr suggests that ~ 100 stars, all with progenitor masses $> 30 M_\odot$, could have undergone SNe in Wd 1, at an average rate of one per 10^4 years (Muno et al. 2006b) over the past million years. The existence of a magnetar in the cluster, with a progenitor mass presumably in excess of $40 M_\odot$ seems to confirm this estimate (Muno et al. 2006a).

Abramowski et al. (2012) reported on the detection of degree-scale very-high-energy (VHE; $E > 100$ GeV) emission from the vicinity of Wd 1 with a total luminosity of $L_{\text{TeV}} \simeq 2 \times 10^{35} (d/4.3 \text{ kpc})^{-2} \text{ erg s}^{-1}$, representing a fraction of $\sim 10^{-4}$ of the total mechanical wind and SN power. Based on the morphological and spectral properties of the H.E.S.S. source (HESS J1646–458) Abramowski et al. (2012) conclude that a significant part of the TeV emission arises from proton-proton interactions of cosmic rays (CRs) accelerated in and around Wd 1 that interact with ambient material. In this scenario an overlap of the VHE γ -ray emission with gas as traced in 21 cm line emission and in CO lines is expected and indeed observed. In a proton-proton scenario a GeV counterpart to the TeV emission is expected with comparable luminosity to the TeV emission and hence detectable with *Fermi*-LAT, albeit with potential different morphology due to energy-dependent diffusion, motivating the study presented here.

2 FERMI-LAT DATA AND ANALYSIS

The Large Area Telescope (LAT) onboard the *Fermi* satellite is a pair-conversion instrument, operating in the 30 MeV to 300 GeV energy range. The point-spread-function (PSF) of the LAT varies with energy and becomes less than 0.5° above ~ 3 GeV (Atwood et al. 2009). The data set analysed here comprises a total of ~ 4.5 years of observations from August 2008 until January 2013. Only photons with energies ≥ 3 GeV are used, greatly reducing the impact of the Galactic diffuse emission on the analysis, minimising the contribution of the bright GeV-detected pulsar PSR J1648–4611 in this region and allowing us to search for multiple, spatially separated components. The *Fermi* Science Tools package v9r27p1 and instrument response functions P7Source_V6 are used. Photons from within a $14^\circ \times 14^\circ$ region centred at the optical Wd 1 position are used in a *binned* maximum likelihood analysis. Sources that are listed in the *Fermi* two-year catalogue (2FGL) and lie within 15° of Wd 1 are modeled. The flux normalisations of objects within 3.5° are left free in the fit, with all other parameters fixed to their 2FGL values. The Galactic diffuse component is modelled using the ring hybrid model gal_2yearp7v6_v0.fits with free normalisation, and the isotropic extragalactic emission and particle background according to the tabulated spectrum of iso_p7v6source.txt.

A search for diffuse HE γ -ray emission from the vicinity of Wd 1 is performed for two different scenarios. First, we assume that all point sources in the 2FGL catalogue *are not* associated to Wd 1 and look for remaining γ -ray emission in the field-of-view. The residual Test-Statistic (TS) map under this hypothesis is shown in Figure 1 (top, right) and shows excess GeV emission south of the stellar cluster. Second, we assume that 2FGL sources that lie within the H.E.S.S. emission region *are* associated to Wd 1 and therefore discard them from the model. The residual GeV emission after excluding 2FGL J1653.9–4627c (S1) and 2FGL J1650.6–4603c (S2), which are both flagged as potentially confused in the 2FGL catalogue, from the source model is shown in the bottom, left panel of Fig. 1. The γ -ray excess is more pronounced than in the first model, offset from Wd 1, and apparently extended with respect to the LAT PSF. These TS maps imply that at least some of the emission attributed to (in particular) S1 in the standard *Fermi* model may be due to a previously unidentified diffuse source in this region.

In the following we test different templates for diffuse γ -ray emission. As significant TeV γ -rays are detected from the vicinity of Wd 1, the VHE γ -ray excess map forms a natural template to test for the GeV signal. The LAT data are not, however, well described by the H.E.S.S. template and an upper limit on the HE γ -ray flux in the TeV emission region can be obtained (see below). The second diffuse model tested is a symmetric two-dimensional Gaussian. A grid-search in position and extension is performed to find the maximum likelihood for such a source model. The best-fit position of this template is at $16^{\text{h}}51^{\text{m}}36^{\text{s}} \pm 24^{\text{s}}$, Dec $-46^\circ 21' 00'' \pm 5'$ (J2000), with a best-fit rms of $\sigma_S = (0.475 \pm 0.05)^\circ$. For the rest of this work we will refer to this source as FGL J1651.6–4621. Including S2 in the source model gives a significantly better fit, suggesting that S2 is a genuine additional point-like γ -ray source, or that the Gaussian template is not an adequate description of the diffuse source morphology. The residual TS map of this model is shown in the bottom, right panel of Fig 1 and illustrates that there is relatively little residual emission from the vicinity of Wd 1 and the Galactic plane in this case. For this source model, the TS of FGL J1651.6–4621 is 173, corresponding to a significance of 13.2σ (pre-trials). As 4820 different combinations of source

Table 1. Fit statistics for different source models. The change in significance of a model is given relative to the next best fit model (i.e. the row above in the table). 2FGL J1653.9–4627c is denoted as S1 and 2FGL J1650.6–4603c as S2. 2FGL - S1 + Gauss, for example, denotes the model which includes the full 2FGL catalogue of point sources *except* S1, plus a Gaussian template with properties described in the text.

Model	$\Delta \log P$	$\sqrt{TS_{\text{model}}}$ σ
2FGL - S1,2	0	
2FGL - S1,2 + H.E.S.S.	4	+2.0
2FGL	75	+8.4
2FGL - S1,2 + Gauss	112	+6.1
2FGL - S1 + Gauss	125	+3.6

position and σ_S have been tested, the post-trials significance is 12.5 standard deviations. The γ -ray spectrum between 3 GeV and 300 GeV for FGL J1651.6–4621 is consistent with a power law in energy with γ -ray index $\Gamma = 2.1 \pm 0.1$ and integral flux $F(>3 \text{ GeV}) = (4.7 \pm 0.5) \times 10^{-9} \text{ ph cm}^{-2} \text{ s}^{-1}$. Note that Neronov & Semikoz (2012) identified significant emission above 100 GeV from a position consistent with this source.

Figure 2 shows the γ -ray spectrum of FGL J1651.6–4621 together with the TeV data of HESS J1646–458. As Abramowski et al. (2012) found no indications for changes in source morphology with energy, we simply scale the total TeV flux by the fractional VHE γ -ray excess to estimate the flux from individual regions. The estimated VHE γ -ray flux from the template region is based on the VHE flux integral within a $1\text{-}\sigma$ radius and corrected for missing flux assuming a Gaussian profile. Fig. 2 also shows LAT upper limits for emission following the H.E.S.S. template, with and without FGL J1651.6–4621 included in the model. The log-likelihood and TS values for the different models tested are listed in Table 1. In an attempt to better describe the diffuse GeV emission, we also tried wedge-shaped Gaussian-like and top-hat templates. Such model fits, however, have lower probabilities than the Gaussian template plus S2. The best-fit γ -ray spectra for more complex templates are systematically steeper, $\Gamma \simeq 2.3$, which could either indicate energy-dependent morphology of the diffuse source, or that S2 is indeed an unrelated (and relatively steep spectrum) point source.

Wd 1 harbours at least 24 Wolf-Rayet stars, two LBV stars and many super- and hyper-giants with a high binary fraction (see Lim et al. 2013, and references therein) of which some show non-thermal emission (Dougherty et al. 2010). As one Colliding Wind Binary (CWB) in the Galaxy is known to emit γ -ray emission, namely η Car (e.g. Reitberger et al. 2012), such emission might be expected from Wd 1. Adding a point-like source at the position of the cluster to the source model does not, however, significantly improve the fit. The 2σ upper limit on the (3–300) GeV cluster γ -ray flux, assuming a γ -ray spectral index of $\Gamma = -2.0$ is found to be $F_{95}(3\text{--}300 \text{ GeV}) < 3.2 \times 10^{-10} \text{ ph cm}^{-2} \text{ s}^{-1}$. The energy output of Wd 1 in γ -ray emission from (3 – 300) GeV is $< 1.5 \times 10^{34} \text{ erg s}^{-1}$. This is a factor of ~ 4 lower than that of η Car ($6 \times 10^{34} \text{ erg s}^{-1}$), tightly constraining the level of particle acceleration in CWBs in this system. There are two known LBV stars in Wd 1 (W9 and W243, e.g. Lim et al. 2013), of which W9 had a mass-loss rate in the recent past comparable to the current mass-loss rate of η Car (Dougherty et al. 2010). The γ -ray limit therefore implies that either one or both of the LBV stars in Wd 1 are not binary systems, or, if they are, that the wind power is much lower

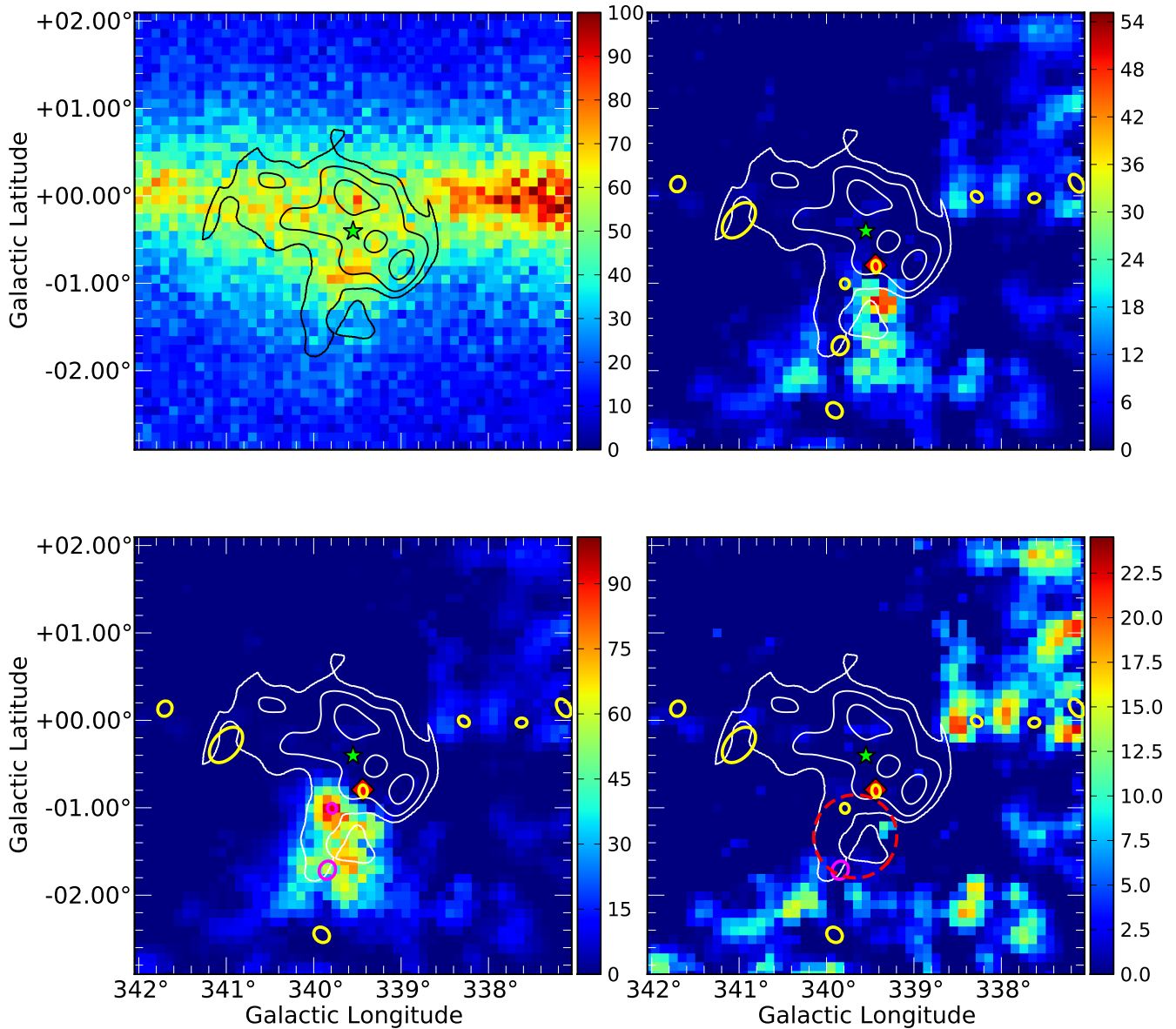


Figure 1. *Fermi*-LAT counts map of the Wd 1 region between 3 GeV and 300 GeV, with H.E.S.S. smoothed excess contours at the 35%, 55%, and 85% of the peak emission overlaid (top, left). The other three panels show residual TS maps in the same energy band. Yellow (magenta) ellipses indicate nearby 2FGL sources that are included (excluded) in the model fits. The green star denotes the Wd 1 stellar cluster position and the red diamond PSR J1648–4611. The residual TS maps show the 2FGL model (top, right), the 2FGL without S1 and S2 model (bottom, left) and the best-fit model using FGL J1651.6–4621 instead of S1 (bottom, right). The red dashed line is the 1- σ variance of FGL J1651.6–4621.

then in η Car or particle acceleration is for some reason much less efficient.

3 DISCUSSION

The dramatically different morphology present in the emission of this region in the GeV and TeV bands implies that either these two sources are unrelated, or that particle transport is playing an im-

portant role. The presence of both a classical young pulsar and a magnetar motivates an exploration of the scenario where the γ -ray emission is dominated by an (electron-accelerating) PWN. Equally, the presence of these stellar remnants implies supernova explosions in the recent past ($\lesssim 10^5$ years ago), which plausibly accelerated protons and nuclei that are now interacting to produce the observed γ -ray emission. Here we discuss these alternatives in turn.

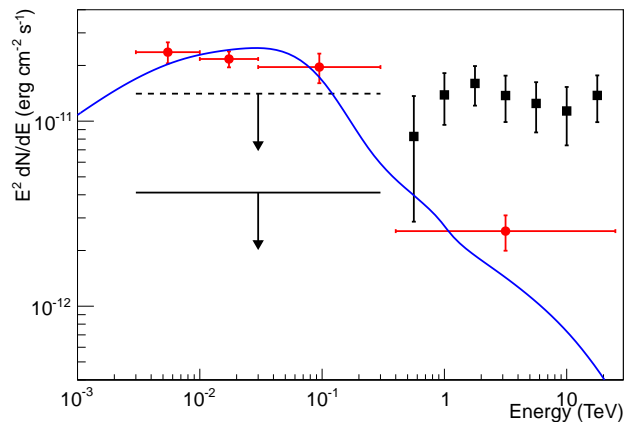


Figure 2. γ -ray spectral energy distributions for two regions close to Wd 1. FGL J1651.6–4621 with TeV flux estimated from H.E.S.S. measurements as described in the text, is shown in red. The γ -ray spectrum of HESS J1646–458 is shown in black. The upper limits on the GeV emission are obtained by excluding (dashed line) and including FGL J1651.6–4621 (solid line) in the model fit. The blue line is an illustrative model curve for IC emission in the PWN scenario discussed in Section 3.1.

3.1 PWN scenario

PWNe form the majority of identified Galactic TeV sources and a small number of GeV associations. The efficient acceleration of particles in PWN is observationally well established with acceleration of e^+/e^- pairs to PeV energies at the termination shock of the relativistic pulsar wind required to explain the radio to VHE γ -ray emission of these objects. The central energy source is a rotating neutron star that converts rotational energy into high-energy particles and subsequently into non-thermal radiation. The energy input to the PWN is a function of time and determined by the spin-down luminosity $\dot{E}(t)$ of the pulsar:

$$\dot{E}(t) = \dot{E}_0 / (1 + t/\tau)^p, \quad \text{with } \tau = P_0 / \dot{P}_0 (n - 1). \quad (1)$$

Here, τ is the characteristic spin-down time, P_0 the pulsar birth period and \dot{P}_0 the first derivative of P_0 . The index p is defined as $p = (n+1)/(n-1)$ and n is the braking index. The injection of energetic particles can be approximated assuming a constant fraction ϵ of \dot{E} is converted to relativistic electrons and positrons.

PSR J1648–4611 is spatially coincident with part of the H.E.S.S. emission and considered as possible counterpart to the VHE signal. The distance of PSR J1648–4611 as derived from dispersion measurements is 5.7 kpc, with an error of $\sim 30\%$ (Kramer et al. 2003), and therefore consistent with the estimated Wd 1 distance. In the following we will consider a physical association of PSR J1648–4611 and Wd 1. The age estimate of PSR J1648–4611 of $\sim 10^5$ years implies that an associated PWN would be in an evolved state and dominated by particles injected early on in its evolution (e.g. de Jager & Djannati-Atai 2009). Observations of PSR J1648–4611 with the Suzaku satellite revealed an extended source in the X-ray data, which is interpreted as a PWN candidate (Sakai et al. 2013) and supports the idea that some of the γ -ray emission might indeed originate in the PWN. Given the proximity to Wd 1, radiation from member stars of the cluster may contribute significantly to the target radiation field for the inverse Compton (IC) process. Assuming a projected distance of $\sim 0.4^\circ$, we estimate that the contribution from Wd 1 is comparable to the typical ISM radiation energy density of ~ 1 eV/cm³. Figure 2 shows the result of

a single-zone, time-dependent model, where particles are injected according to Equation 1 (e.g. Funk et al. 2007). For the measured current spin period $P_{\text{now}} = 165$ ms, the inferred characteristic age of 110 kyr (Manchester et al. 2005) and an assumed conversion efficiency ϵ of 20%, a pulsar birth period of $P_0 = 21$ ms is required to match the GeV flux. The radius of the GeV emission region assuming a 4.3 kpc distance is ~ 40 pc, comparable to the extension of HESS J1825–137 at these energies (Grondin et al. 2011). However, due to significant IC cooling on the stellar cluster plus ISM plus CMB radiation fields, it is very difficult to accommodate the TeV emission in the same scenario. This emission could be attributed to (possibly multiple) additional (much younger) PWNe, which have not so far been observed.

3.2 SNR/proton scenario

Given the presence of target material in the vicinity, and the likely local acceleration of protons and nuclei in either supernova explosions or cluster winds, a π^0 -decay explanation for some or all of the γ -ray emission is attractive. Making quantitative predictions in this scenario, with which to compare the observations, is however rather difficult: the three dimensional distribution of both the CRs and target material must be modelled or assumed. The distribution of target material can be estimated from atomic hydrogen (HI) and CO maps, but with considerable uncertainties on the distribution of material along the line-of-sight and/or the presence of dense or ionised material that could be missed. The distribution of CRs is hard to predict due to: 1) uncertainties in the injection spectrum, location and time for the CRs and 2) uncertainties on their subsequent propagation. These uncertainties exist in essentially all diffuse γ -ray sources, but are exacerbated in this case by the likely presence of significant bulk motions (advection) as well as energy-dependent and presumably environment dependent diffusion. Nevertheless, we attempt here to construct a scenario which is consistent with the observational data, as an illustration of the kind of situation we may be dealing with here, which could be constrained by a future precision γ -ray instrument such as CTA, and to provide a reasonable estimate of the required energy input.

Figure 3 shows the ¹²CO emission from this region, tracing molecular hydrogen, with H.E.S.S. contours and best-fit *Fermi* ellipse superimposed. Three features/regions are apparent in this map in the immediate vicinity of Wd 1:

- A** – a relatively low-density region to the south of Wd 1
- B** – a molecular cloud complex coincident with the TeV peak
- C** – the prominent star-forming region G340.2–0.2.

These regions have been investigated in terms of their HI emission as well as CO, in order to provide density estimates. Integrating in the velocity range -58.5 km s⁻¹ to -52.0 km s⁻¹ and using conversion factors of $X_{\text{HI}} = 1.8 \times 10^{18}$ cm² / (K km s⁻¹) (Yamamoto et al. 2003) and $X_{\text{CO} \rightarrow \text{H}_2} = 1.5 \times 10^{20}$ cm² / (K km s⁻¹) (Strong et al. 2004), we find total cloud masses between $\sim (2-7) \times 10^5 M_\odot$ (Table 2). The velocity range has been chosen following Abramowski et al. (2012) and to account for possible local gas motions of several km s⁻¹.

Given the possibility of different diffusion coefficients and even different transport mechanisms in different regions, and the rather complex geometry, we adopt a Monte-Carlo approach to the particle transport. Three distinct zones are defined in which transport properties and local density differ, corresponding approximately to the regions A, B and C discussed above. Particles (2000 per energy bin, with 20 energy bins per decade) are injected at the

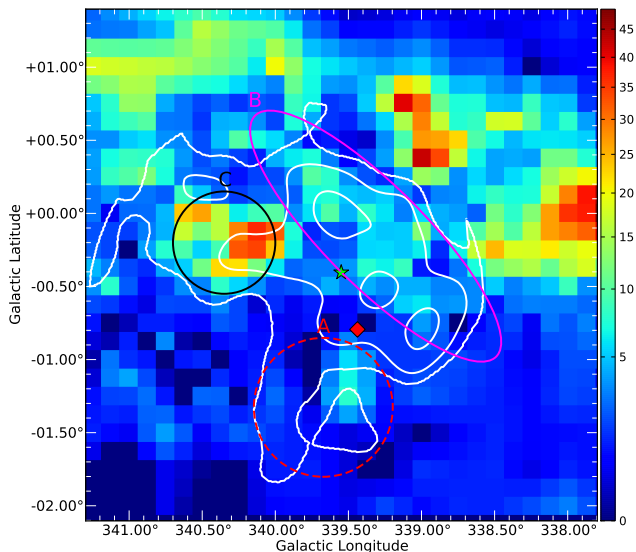


Figure 3. ^{12}CO map from Dame et al. (2001), integrated in the velocity range -58.5 km s^{-1} to -52.0 km s^{-1} . Smoothed H.E.S.S. excess contours and markers are as described in Fig 1. Regions A,B, and C are used to estimate the H_2 and HI masses and densities given in Table 2.

Table 2. Mass estimates for neutral and ionised hydrogen in the regions defined in Fig 3. The average gas density estimates rely on the assumed three-dimensional structure and are therefore uncertain by a factor ~ 2 .

Region	M_{H_2} $10^5 M_\odot$	M_{HI} $10^5 M_\odot$	\bar{n}_{H} cm^{-3}
A	0.9	1.0	5
B	3.4	4.2	10
C	4.0	1.2	35

position of Wd 1 and followed for $t_s = 10^5$ years, or until they leave the region of interest. The nominal 10^5 year age is comparable to the characteristic age of the magnetar (1.7×10^5 years), but significantly older than the estimated mean time between SN explosions in the cluster ($\sim 10^4$ years). In each 100-year time-step the particles are considered to propagate by diffusion, resulting in a random rms displacement of $\sqrt{6D(E, \mathbf{r})dt}$, where $D(E, \mathbf{r})$ is the energy and position (zone) dependent diffusion coefficient, with a superimposed motion with fixed velocity and direction for those particles in zone A, away from a point at the northern edge of this zone. The energy dependence of the diffusion coefficient is assumed to be $D(E) = D_{10}(E/10 \text{ GeV})^\delta$, with a (conventional) value of $\delta = 0.6$ adopted. Smaller values of δ , however, make it hard to explain the energy-dependent morphology observed. Different values of D_{10} are tested in different zones. At the end of the propagation simulation, particle weights are multiplied by the local density and integrated in the line-of-sight direction, to provide a map of integrated (CR density \times gas density) which can be used for the calculation of the γ -ray flux. The parameterisations of Kamae et al. (2006) are used to calculate the γ -ray emission expected from each map pixel and finally the γ -ray SED is integrated in each of regions A, B and C.

Figure 4 shows the result of two sets of such simulations, which are consistent with the available measurements and upper limits in the three zones. To provide a reasonable match to the observations within this framework we require:

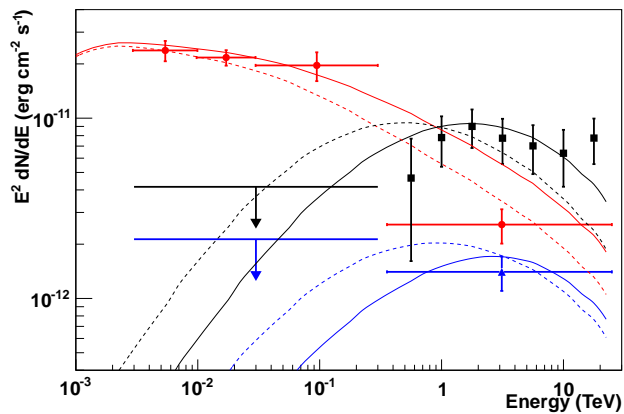


Figure 4. Illustrative model curves for diffusing protons compared to the measured spectral energy information for regions A, B and C described in the text. Red points (circles) and curves correspond to region A, black (squares) to region B and blue (triangles) to region C. The black data points are taken from Abramowski et al. (2012) and scaled down by the fractional excess contained in region A. The blue and red points are derived as described in Section 2. The blue limit is derived by assuming an additional point source at the position of G340.2–0.2. Dashed model curves have diffusion coefficients D_{10} of $2 \times 10^{25} \text{ cm}^2 \text{ s}^{-1}$ (A and C) and $2/3 \times 10^{25} \text{ cm}^2 \text{ s}^{-1}$ (B). The injection spectrum of relativistic protons follows a power law with index -2.05 , with a total of 1.1×10^{51} ergs injected. The solid curves are identical except for a decrease of D_{10} in all regions by a factor 2.

- Significantly slower diffusion than the typical values inferred for GCRs, and different diffusion speeds in Zones A and B. The conventional Galactic D_{10} is $10^{28} \text{ cm}^2 \text{ s}^{-1}$. Values closer to $10^{25}(t_s/10^5 \text{ yr})^{-1} \text{ cm}^2 \text{ s}^{-1}$ are required here, with factor ~ 3 slower diffusion into the molecular clouds of Zone B. Such adjustments to the standard paradigm are uncomfortable, but the situation may overall be rather similar to that in W 28 (e.g. Fujita et al. 2009; Ohira et al. 2011; Li & Chen 2012), particularly for a SN explosion $\sim 10^4$ years ago.

- A bulk flow with $v \sim 400 \text{ km/s}$ towards the South (in Zone A) that corresponds to a 1° offset from the cluster for material carried by the flow for $\sim 10^5$ years. Such an outflow from the cluster seems plausible given the stellar population of Wd 1 and might be similar (in speed) to the winds observed in Starburst galaxies such as NGC 253 (e.g. Zirakashvili & Völk 2006).

- An injection spectrum close to E^{-2} .
- $\sim 10^{51}$ erg injected in relativistic protons and nuclei.

Such a solution is certainly not unique, the problem being rather unconstrained by the available, rather low resolution, γ -ray data, and of course the time(s) at which particles are injected are highly uncertain. The propagation scenario does however seem plausible. The primary difficulty is the energy required in protons, which is close to 10^{51} ergs for all models which provide reasonable agreement with the data, constrained by the GeV flux and density in region A. Multiple SNR and/or an extremely energetic event, both of which seem plausible for Wd 1, would be required.

4 CONCLUSIONS AND OUTLOOK

We have established the existence of a new GeV source in the vicinity of the massive stellar cluster Wd 1. The emission is extended in

nature and likely associated to the cluster either directly, via collective wind effects, or indirectly via PWN(e) and/or SNR(s). A single or multiple PWNe can naturally explain the GeV emission but would leave the TeV emission unexplained. A scenario in which protons from a single very energetic SNR or multiple SNRs diffuse away from Wd 1 and interact with the environment has been investigated here and can plausibly explain the γ -ray data with a required energy input of $\sim 10^{51}$ erg. Wd 1 is the most massive stellar cluster in the Galaxy hosting a magnetar and a rich population of evolved massive stars. These unique characteristics imply that the SNR progenitor stars had very high masses, i.e. $\gtrsim 40 M_{\odot}$, and that the associated SN explosions may well have been very energetic. This in turn could explain the large energy required in the scenario we employ here. A detailed investigation of the underlying particle acceleration, propagation and interaction processes, however, is limited by the low resolution of γ -ray and CO data. To study this complex and important region in more detail, requires high resolution, more sensitive γ -ray instruments such as CTA as well as spatial X-ray coverage and high-resolution radio data. Especially CTA with its wider field-of-view and factor 5 better PSF will be crucial to study the connection between the *Fermi* and H.E.S.S. emission.

ACKNOWLEDGEMENTS

The authors would like to thank the anonymous referee for his useful comments and Thierry Montmerle for fruitful discussions. This work has made use of public *Fermi* data and Science Tools provided by the Fermi Science Support Centre. S.O. acknowledges support from the Humboldt foundation by a Feodor-Lynen fellowship.

REFERENCES

- Abramowski A. et al., 2012, *A&A*, 537, A114
 Abramowski A. et al., 2011, *A&A*, 525, A46+
 Ackermann M. et al., 2011, *Science*, 334, 1103
 Aharonian F. et al., 2005, *A&A*, 431, 197
 Aharonian F. et al., 2007, *A&A*, 467, 1075
 Atwood W. B. et al., 2009, *ApJ*, 697, 1071
 Bykov A. M., 2001, *Space Science Reviews*, 99, 317
 Clark J. S., Negueruela I., 2002, *A&A*, 396, L25
 Clark J. S., Negueruela I., Crowther P. A., Goodwin S. P., 2005, *A&A*, 434, 949
 Dame T. M., Hartmann D., Thaddeus P., 2001, *ApJ*, 547, 792
 de Jager O. C., Djannati-Ataï A., 2009, in *Astrophysics and Space Science Library*, Vol. 357, *Astrophysics and Space Science Library*, Becker W., ed., p. 451
 Dougherty S. M., Clark J. S., Negueruela I., Johnson T., Chapman J. M., 2010, *A&A*, 511, A58
 Fujita Y., Ohira Y., Tanaka S. J., Takahara F., 2009, *ApJ*, 707, L179
 Funk S., Hinton J. A., Pühlhofer G., Aharonian F. A., Hofmann W., Reimer O., Wagner S., 2007, *ApJ*, 662, 517
 Grondin M.-H. et al., 2011, *ApJ*, 738, 42
 Kamae T., Karlsson N., Mizuno T., Abe T., Koi T., 2006, *ApJ*, 647, 692
 Kramer M. et al., 2003, *MNRAS*, 342, 1299
 Li H., Chen Y., 2012, *MNRAS*, 421, 935
 Lim B., Chun M.-Y., Sung H., Park B.-G., Lee J.-J., Sohn S. T., Hur H., Bessell M. S., 2013, *AJ*, 145, 46
 Manchester R. N., Hobbs G. B., Teoh A., Hobbs M., 2005, *AJ*, 129, 1993
 Muno M. P. et al., 2006a, *ApJ*, 636, L41
 Muno M. P., Law C., Clark J. S., Dougherty S. M., de Grijs R., Portegies Zwart S., Yusef-Zadeh F., 2006b, *ApJ*, 650, 203
 Neronov A., Semikoz D. V., 2012, *Phys. Rev. D*, 85, 083008
 Ohira Y., Murase K., Yamazaki R., 2011, *MNRAS*, 410, 1577
 Parizot E., Marcowith A., van der Swaluw E., Bykov A. M., Tatischeff V., 2004, *A&A*, 424, 747
 Reitberger K., Reimer O., Reimer A., Werner M., Egberts K., Takahashi H., 2012, *A&A*, 544, A98
 Sakai M., Matsumoto H., Haba Y., Kanou Y., Miyamoto Y., 2013, *ArXiv e-prints*
 Strong A. W., Moskalenko I. V., Reimer O., Digel S., Diehl R., 2004, *A&A*, 422, L47
 Yamamoto H., Onishi T., Mizuno A., Fukui Y., 2003, *ApJ*, 592, 217
 Zirakashvili V. N., Völk H. J., 2006, *ApJ*, 636, 140